© 2024

EXCITATION OF WANNIER – STARK STATES IN A CHAIN OF COUPLED OPTICAL RESONATORS WITH LINEAR GAIN AND NONLINEAR LOSSES

A. Verbitskiy[*], *A. Yulin*

School of Physics and Engineering, ITMO University
197101, St. Petersburg, Russia

In this paper, we theoretically study the nonlinear dynamics of Wannier – Stark states in a dissipative system of interacting optical resonators whose resonant frequencies depend linearly on their number. We show that negative losses in some resonators can switch the system to a lasing regime with Wannier – Stark states acting as working modes. Our extensive numerical simulations show that single-frequency stationary regimes can exist in such a system as well as multi-frequency ones. In the latter case, Bloch oscillations can appear in the system. We investigate selective excitation of Wannier – Stark states enabled by an appropriate dissipation profile. A simple perturbation theory describing the quasi-linear regimes is developed and compared with the numerical results.

1. INTRODUCTION

Wannier – Stark ladders (WSLs) continue to be of great interest to scientists in different areas of physics, such as solid-state physics, condensed matter, and quantum magnets [1–3]. The WSL effect consists in the presence of equidistant lines in the spectrum, which correspond to the eigenmodes of the system (Wannier – Stark states) [4,5]. Beating between these states in time may result in periodic motion, i.e. Bloch oscillations (BOs) [6–8].

BOs were first predicted in solid-state physics. However, their experimental observation in solids is quite challenging, and it took many years to confirm the effect experimentally [9]. BOs turned out to be a very common phenomenon, and they were found in a large variety of physical systems such as atomic systems [10–15], lasers [16], coupled LC circuits [17], mechanical systems [18–21], and plasmonic [22–27] or exciton-polariton systems [28–30].

The advantage of optical systems over solid-state ones is that optical experiments for observation of the aforementioned effects are more feasible. Therefore, theoretical prediction of optical WSLs and BOs [31–42] was quickly followed by experimental demonstrations.

One of the first experimental observations of an optical WSL was reported in [43]. Here, the Wannier – Stark (WS) states are realized using a chirped Moire grating. Another evidence of the existence of WSLs is presented in the work [44], where a spatial tilt of the minibands occurs due to a linear gradient of the optical thickness of the superlattice layers. In addition, WS states were observed in photonic lattices formed in a photorefractive material using relatively strong light. For this purpose, the formed lattices were irradiated with laser beams with a WS profile retrieved from a hologram [45]. Moreover, strongly localized WS states in a curved photonic lattice were obtained due to a large gradient of the refractive index and weak interaction between the waveguides [46]. BOs were also experimentally detected in the optical range, see, for example [47,48]. In these works, under the influence of temperature or by changing the waveguides' width, a linear gradient of the refractive index was created in a waveguide array, which led to periodic spatial oscillations of the light beam due to Bragg and total internal reflections

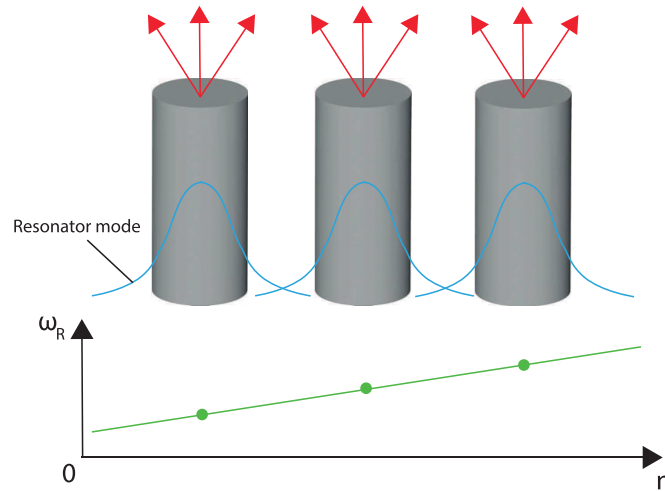[*] E-mail: alexey.verbitskiy@metalab.ifmo.ru

Fig. 1. (Color online) Sketch of the considered system

at the opposite edges of the array. In addition, BOs were observed in porous silicon structures, in which, to incline the optical band authors used a cavity whose width increased linearly across the structure [49, 50]. Besides, by bending a waveguide array, BOs can also be achieved in optical systems [51–53]. Another important system supporting BOs are parity-time synthetic photonic lattices [54, 55]. A comprehensive review of the research on BOs and related phenomena is provided in [56].

The presence of dissipation, pump, and nonlinear effects in optical systems (for example, arrays of interacting nonlinear optical cavities) calls for generalization of the BOs theory to nonlinear dissipative systems. Let us note that optical systems such as microlaser arrays are promising sources of coherent radiation [57–62]. Thus, the study of these systems is not only of fundamental, but also of practical interest.

Active systems of microcavities with WS states and BOs have not yet been realized experimentally. However, currently, other optical and waveguide systems are actively studied in practice, in which interesting phenomena from the physics of WS states are also observed [21, 30, 63]. These advances in not only theoretical but also experimental demonstration of BOs in different optical systems stimulate further research of this effect in photonics and, in particular, in laser systems.

Experimental implementation of microlaser systems with WS modes is indeed not an easy task. First, the manufacturing of such systems requires cutting-edge precise technologies that are not readily available. Second, the quality factors of typical optical microresonators are low, and thus, high linear gain is required

to achieve lasing in these resonators. These are serious issues, but the advances of modern technologies allow us to expect that systems with the required parameters could be manufactured in near future. In particular, new materials such as perovskites demonstrate fascinating properties in laser devices [60], including very high linear gain. Dielectric resonators with a high quality factor based on bound states in the continuum (BICs), which have been actively developed recently [64, 65], are another promising platform for creating active microresonators with WS modes. The third possible platform for experimental observation of BOs is polariton lasers based on micropillars [66]. Considering these prospects, theoretical investigation of optical systems supporting WS states and BOs is of great physical interest, and the respective theoretical findings can boost further experimental activity in this direction.

In this paper, we aim to study the nonlinear dynamics of WS states in one-dimensional systems of coupled optical cavities, in which each of the resonators supports only one mode defined by the material and geometry of the resonator. The described system is schematically shown in Fig. 1. To obtain a Bloch-type system, we introduce linear dependence of the cavities' frequency on their index (i. e., number). A similar system driven by a train of coherent laser pulses is considered in [67], where the resonant excitation of WS modes and chaotic BOs were demonstrated. The present paper is focused on the dynamics of WS states in microlaser arrays with population inversion created either by optical or electric pump.

Below, we consider in detail different regimes of WS lasers, their switching from single-frequency to multi-

frequency regimes, and the appearance of BOs. To explain the behaviour of such systems near the lasing threshold, we develop a perturbation theory. We consider this work as a proof of concept rather than a discussion of the optimal experimental system, and, therefore, we choose the simplest lasing cavity model. We should acknowledge that for a real experiment, the scheme and, consequently, the theoretical model might require elaboration.

To describe the dynamics of light in microresonators, we use a well-known discrete model for slowly varying complex amplitudes $U_n(t)$ of the modes of individual resonators [68–79]:

$$i\partial_t U_n + \sigma(U_{n+1} + U_{n-1}) + \mu n U_n + i\gamma_n U_n + \\ + i\beta_n |U_n|^2 U_n = 0, \quad (1)$$

where n is the index enumerating the resonators, σ is the coupling strength between the resonators, μ accounts for the dependence of the resonant frequency on the resonator index, and γ_n and β_n are the linear and nonlinear losses, respectively. Both γ_n and β_n can differ for different resonators. Let us note that here we consider a simple, but physically meaningful case: we assume that the nonlinear effects change the effective losses, but not the resonant frequencies of the individual resonators. We acknowledge that nonlinear correction of the resonant frequencies can be of importance, but it requires a special consideration, which will be done elsewhere.

A sufficiently strong incoherent pump can not only change the linear losses, but also make them negative. Thus, such a pump can transform an individual cavity into a laser. However, as we consider a system of resonators, we need to calculate the effective gain of the supermodes of the system rather then the effective gain of individual resonators. For a rough estimate, we can consider the stationary states as a balance between the effective gain and effective nonlinear losses calculated for the WS state. Importantly, nonlinear losses might be present only in the pumped cavities, or in all the resonators. Further, we will show that in these two cases, the WS modes' dynamics is different.

The parameters of a coupled waveguide array differ depending on their experimental implementations. We use typical data from work [47]: $\sigma = 125$ m^{-1}, $\mu = 25$ m^{-1}, and $\gamma \approx 0.5$ dB/cm, suitable for demonstrating the discussed effects. However, the value of linear losses γ in this work is significantly higher than we need. In practice, this circumstance can be overcome by using high-Q BIC-based systems [64, 65]. We also assume the nonlinear parameter β to be equal to

125 m^{-1}, which is determined by the effect of gain saturation and selection of the appropriate absorber. For the sake of mathematical convenience, we normalize the coefficients of the equation (1) by the strength of the coupling between the neighboring resonators σ, and as a consequence, we obtain normalized time t, $\sigma = 1$, $\mu = 0.2$, and $\beta = 1$. We choose $\gamma = 0.01$ as an appropriate value for linear losses.

The paper is structured as follows. For a systematic study of the problem, we start with the simplest case, in which only one resonator is pumped (Section 2 of the paper). In Section 3, we show that simultaneous excitation of several resonators makes the system's dynamics richer, giving rise to multi-frequency regimes, including self-sustained BOs. In Section 4, mode selection is considered. We show that the efficiency of mode excitation depends on the pump profile, and by controlling the pump shape, we can extend the range of intensities where the single-frequency regime takes place. The main findings of the work are briefly discussed in the Conclusion.

2. SYSTEMS EXCITED BY LINEAR GAIN IN ONLY ONE RESONATOR

We start with a simple case where γ_n is negative in only one resonator with $n = 0$, and in all other resonators, γ_n is a positive constant. This means that we have a linear amplification in the resonator $n = 0$, and the other resonators have linear losses.

We choose the linear losses to be $\gamma_n = \gamma$ for $n \neq 0$ and $\gamma_0 = \gamma - a$, where a is the pump amplitude, and study the dynamics of the system numerically. Our numerical simulations reveal that only the trivial solution $U_n = 0$ is possible as long as the linear gain a is lower than the lasing threshold, which depends on the parameters of the system γ and μ. If the gain exceeds the threshold, the eigenmodes emerge in the system. If the dissipative and nonlinear terms are small, then these emerging modes can be very accurately approximated by the WS states, which are known analytically for the equation (1) in the conservative limit $\gamma_n \to 0$, [33]. The eigenvalues of the WS states form an equidistant spectrum $\omega_m = \mu m$ with eigenfunctions

$$W_{n-m} = J_{n-m}\left(\frac{2\sigma}{\mu}\right),$$

where the index m enumerates the eigenstates. We use WS states normalized so that
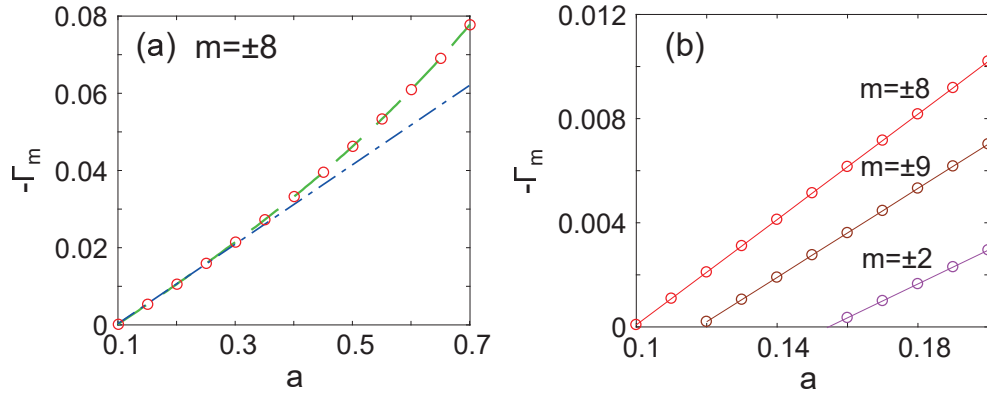
$$\sum_n W_{n-m}^2 = 1.$$

Fig. 2. (Color online) a — Effective linear gains $-\Gamma_m$ of the Wannier−Stark states with the fastest-growing amplitudes ($m = \pm 8$) vs. the pump amplitude a: obtained by numerical simulation (red circles), the perturbation method (dash-dotted blue line), and the eigenvalues (dashed green line). b — Effective linear gains $-\Gamma_m$ of Wannier−Stark states with $m = \pm 8$ (red circles), $m = \pm 9$ (brown circles), and $m = \pm 2$ (magenta circles) vs. the pump amplitude a, obtained by numerical simulation. The solid lines are guides for eyes. The used parameters are: $\mu = 0.2$, $\gamma = 0.01$

If the dissipation is so low that it does not affect the spatial structure of the eigenstates, a simple perturbation theory can be developed. The quantity

$$E = \sum_n |U_n|^2$$

(energy of the field in the system) is conserved if $\gamma_n = 0$ and $\beta_n = 0$. If γ_n and β_n are nonzero, but small, the field in the system can be found in the form

$$U_n^{(m)} = A_m(t)W_{n-m}\exp(i\mu m t),$$

where $A_m(t)$ is the time-dependent complex amplitude of the m-th WS state. Substituting this into (1), multiplying by W_{n-m}, and calculating the sum over n, we obtain ordinary differential equations for A_m:

$$\partial_t A_m = -\Gamma_m A_m - \mathcal{B}_m|A_m|^2 A_m, \qquad (2)$$

where

$$\Gamma_m = \sum_n \gamma_n W_{n-m}^2, \quad \mathcal{B}_m = \sum_n \beta_n W_{n-m}^4$$

are the effective linear and nonlinear losses for the m-th mode.

For a purely dissipative nonlinearity (i. e., affecting only the effective losses, but not the resonant frequency of the cavities), the equations (2) can be re-formulated as a set of equations for the intensities $I_m = |A_m|^2$:

$$\partial_t I_m = 2(-\Gamma_m I_m - \mathcal{B}_m I_m^2). \qquad (3)$$

For our choice of $\gamma_n = \gamma - a\delta_{0n}$ (δ_{ij} is the Kronecker symbol), the sum in the expression for the effective linear losses Γ_m can be easily calculated analytically:

$$\Gamma_m = \gamma - aW_{-m}^2. \qquad (4)$$

The intensity distributions of the WS states are symmetric and have two main maxima, located symmetrically with respect to the center of the mode. Therefore, if the system is excited by linear gain only in one resonator, then there are two modes with the fastest-growing amplitudes and the same increment. For the parameters used in the numerical simulations, the indexes of such modes are $m_{max} = \pm 8$.

Now let us compare the results of the perturbation theory with those of the direct numerical simulations of the master equation (1). It is natural to introduce the effective linear gain of a mode as $-\Gamma_m$. Figure 2 a shows the effective linear gains extracted from the numerical simulations and calculated by formula (4) as functions of the pump amplitude a. One can see that in the vicinity of the lasing threshold, where the dissipative terms can be considered as small corrections, the results of the perturbation theory are in very good agreement with the numerical simulations.

The complex frequencies of the modes can also be found by analyzing the linearized equation for the amplitudes U_n:

$$i\partial_t U_n + \sigma(U_{n+1} + U_{n-1}) + \mu n U_n + i\gamma_n U_n = 0. \quad (5)$$

Then, by choosing a solution in the form

$$U_n(t) = V_n \exp(i\omega t),$$

we obtain an eigenvalue problem:

$$\omega V_n = \sigma(V_{n+1} + V_{n-1}) + \mu n V_n + i\gamma_n V_n. \qquad (6)$$

The real part of ω is the eigenmode frequency, the imaginary part is its dissipation rate, and the eigenvector V_n describes the structure of the eigenmode. If there are no dissipative terms, the eigenstates are the conservative WS states discussed above. The solution of the spectral problem allows us to find the exact solutions for the eigenstates in the dissipative case. We solved the spectral problem numerically to confirm that the dissipative terms do not significantly affect the structure of the eigenmodes.

Comparing effective linear gains of different WS states can also be useful. The numerically found $-\Gamma_m$ for the six modes with the fastest-growing amplitudes are shown in Fig. 2 b as a function of the pump amplitude a. One can see that for our parameters, the modes with the fastest-growing amplitudes and the lowest lasing threshold are the modes with $m = \pm 8$; the second and the third fastest-growing modes have the indexes $m = \pm 9$ and $m = \pm 2$, respectively.

The intensity of the stationary states $\overline{I_m}$ formed in the system can be easily found from (3):

$$\overline{I_m} = \frac{-\Gamma_m}{\mathcal{B}_m}. \tag{7}$$

Figure 3 shows the dependencies of the stationary intensities of three pairs of WS states with the highest effective linear gains on the pump a for two cases: (a) when the nonlinear losses are nonzero only in the excited resonator with $n = 0$: $\beta_0 = \beta$ and (b) for spatially uniform nonlinear losses: $\beta_n = \beta$. The stationary intensities can be higher for the modes with lower effective linear gains, see Fig. 3 a. The possible reason is, if the nonlinear losses are nonzero only in the excited resonator, the modes with the highest effective linear gains have the highest nonlinear losses, and their ratio (7) is lower than that of the modes with the lower effective linear gains.

Our numerical simulations reveal that for small pump intensities, only one pair of the WS states with the highest effective linear gain is dynamically stable. The dependencies of the stationary intensities of the WS states extracted from the numerical simulations are shown in Fig. 3. The perturbation theory and the numerical simulations are in good agreement for low pump intensities.

It can be interesting to study the dynamics when the initial conditions have the form of low-intensity noise. As we mentioned above, the modes are formed when the pump exceeds a certain threshold. We choose the pump exceeding only the threshold for the modes with the largest increment. Thus, for the parameters we chose, only the amplitudes of the modes $m = \pm 8$

grow. The numerical simulations show that if there are nonlinear losses only in the pumped resonator, a single-frequency stationary state is formed as a WS state with $m = 8$ or $m = -8$. The probability of the formation of each of the states is $1/2$. The formation of the stationary states is illustrated in Fig. 4 a, b, d and e.

If nonlinear losses are distributed evenly in the system, there are different regimes of stationary states formation. The excitation thresholds, of course, remain the same, but the stationary state forming from a weak noise varies periodically in time. Very close to the excitation threshold, the stationary state can be considered as a superposition of the WS states with $m = 8$ and $m = -8$; consequently, the stationary state contains temporal harmonics with frequencies equal to the WS states' eigenfrequencies. The formation of such a state is illustrated in Fig. 4 c, f.

To explain such a behaviour of the system, we expand the perturbation theory described above by writing the equations for the amplitudes $A_\pm$ of two interacting modes $m = \pm \tilde{m}$ with the highest effective linear gains. Thus, we seek the field in the form

$$U_n = A_+ W_{n-\tilde{m}} \exp(i\tilde{m}t) + A_- W_{n+\tilde{m}} \exp(-i\tilde{m}t).$$

Substituting this ansatz into (1) and projecting the equation on the eigenstates, we obtain equations for $A_\pm$. These equations can be reduced to equations for the intensities $I_\pm$ in a similar way to (3):

$$\partial_t I_+ = -2(\Gamma + \mathcal{B}I_+ + \tilde{\mathcal{B}}I_-)I_+, \tag{8}$$

$$\partial_t I_- = -2(\Gamma + \mathcal{B}I_- + \tilde{\mathcal{B}}I_+)I_-, \tag{9}$$

where

$$\tilde{\mathcal{B}} = 2\sum_n \beta_n W_{n-\tilde{m}}^2 W_{n+\tilde{m}}^2, \quad \Gamma = \Gamma_{\pm\tilde{m}}.$$

As we derived these equations, we assumed that the difference between the eigenfrequencies of these states is large, and we can safely neglect the quickly oscillating terms.

Let us analyse the fixed points of the dynamical system (8)–(9). For $\Gamma > 0$, there is only a trivial solution $I_\pm = 0$. For negative losses (and, correspondingly, positive gain), there are four solutions:

$$I_\pm = 0;$$

$$I_+ = 0, \quad I_- = \frac{-\Gamma}{\mathcal{B}};$$

$$I_- = 0, \quad I_+ = \frac{-\Gamma}{\mathcal{B}};$$

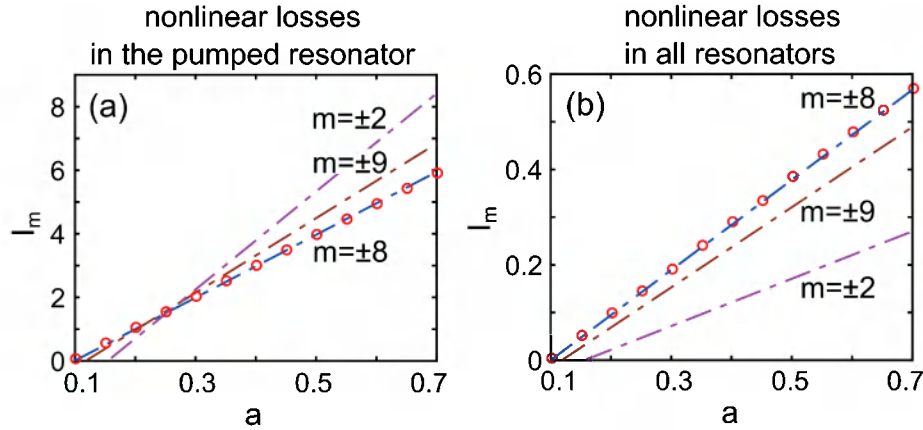$$I_\pm = \frac{-\Gamma}{\mathcal{B} + \tilde{\mathcal{B}}}.$$

Fig. 3. (Color online) Stationary intensities I_m of different Wannier–Stark states vs. the pump amplitude a, obtained with the perturbation method (dash-dotted lines) and by numerical simulation (circles) for (a) nonzero nonlinear losses only in the excited resonator with $n = 0$, i. e., $\beta_0 = \beta$, and (b) spatially uniform nonlinear losses, i. e., $\beta_n = \beta$. The used parameters are: $\mu = 0.2$, $\gamma = 0.01$, $\beta = 1$
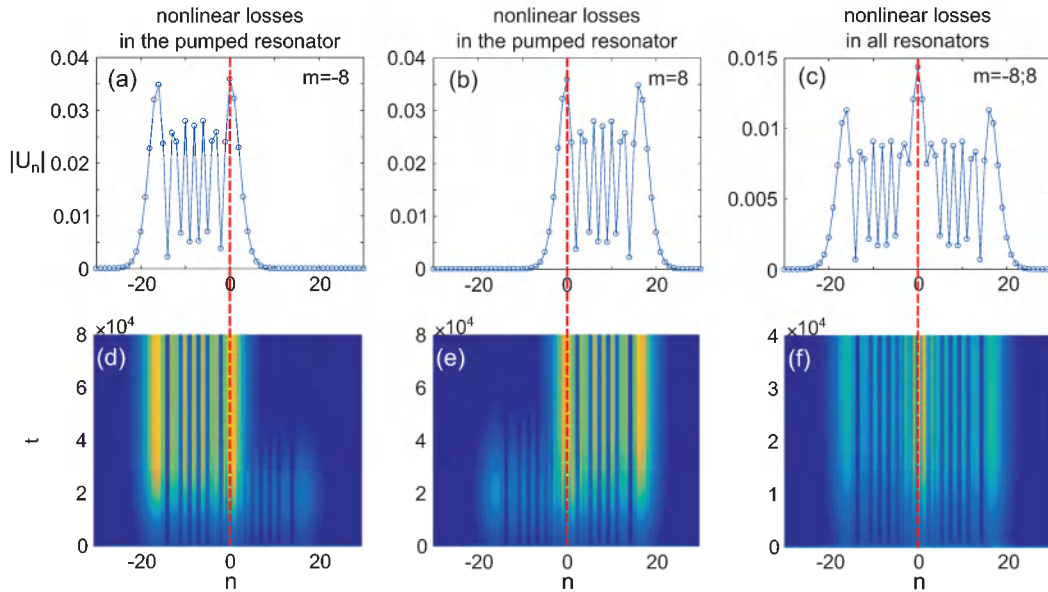

Fig. 4. (Color online) Stationary states $|U_n|$ in the form of WS states with $m = -8$ (a), $m = 8$ (b), $m = -8$ (c) and $m = 8$ (time-averaged field); figs. d, e and f show the respective evolutions of the field module $|U_n(t)|$. The pump amplitude slightly exceeds the excitation threshold. Nonlinear losses are nonzero only in the excited resonator with $n = 0$, i.e., $\beta_0 = \beta$, for a, b, d, and e; nonlinear losses are spatially uniform, i.e., $\beta_n = \beta$, for c and f. The blue circles correspond to the resonators, the solid blue lines are guides for eyes, and the dashed red lines correspond to the pumped resonator with $n = 0$. The used parameters are: $\mu = 0.2$, $\gamma = 0.01$, $a = 0.1$, $\beta = 1$

We can directly explore the stability of these states by writing linearized equations for small perturbations $\xi_\pm$ of the intensities $I_\pm$ and finding the eigenvalues governing the evolution of the perturbations. The trivial state is, of course, always unstable $\lambda_{1,2} = -2\Gamma$. The second and the third states have the eigenvalues $\lambda_1 = -2\Gamma(1 - \tilde{\mathcal{B}}/\mathcal{B})$ and $\lambda_2 = 2\Gamma$; λ_2 is always negative

for $\Gamma < 0$, λ_1 is negative for $\mathcal{B} < \tilde{\mathcal{B}}$ and positive otherwise. Therefore, this state can be either a stable node for $\mathcal{B} < \tilde{\mathcal{B}}$ or a saddle for $\mathcal{B} > \tilde{\mathcal{B}}$. The last state

$$I_\pm = \frac{-\Gamma}{\mathcal{B} + \tilde{\mathcal{B}}}$$

has the eigenvalues

$$\lambda = \frac{2\Gamma}{\mathcal{B} + \tilde{\mathcal{B}}}\left(\mathcal{B} \pm \tilde{\mathcal{B}}\right).$$

From this, we can conclude that this state is stable (a stable node) for $\mathcal{B} > \tilde{\mathcal{B}}$ or unstable (saddle) for $\mathcal{B} < \tilde{\mathcal{B}}$.

Thus, the stability analysis tells us that if $\mathcal{B} > \tilde{\mathcal{B}}$, then for the system (8)–(9), there is only one stable stationary state,

$$I_\pm = \frac{-\Gamma}{\mathcal{B} + \tilde{\mathcal{B}}}.$$

For $\mathcal{B} < \tilde{\mathcal{B}}$, there are two stable states:

$$I_+ = 0, \quad I_- = \frac{-\Gamma}{\mathcal{B}},$$

and

$$I_+ = \frac{-\Gamma}{\mathcal{B}}, \quad I_- = 0.$$

Now let us estimate the values $\tilde{\mathcal{B}}$ and $\mathcal{B}$. When only $\beta_0 \neq 0$, then

$$\mathcal{B} = \sum_n \beta_n W_{n-\tilde{m}}^4 = W_{\tilde{m}}^4$$

and

$$\tilde{\mathcal{B}} = 2\sum_n \beta_n W_{n-\tilde{m}}^2 W_{n+\tilde{m}}^2 = 2W_{\tilde{m}}^4.$$

This means that $\tilde{\mathcal{B}} = 2\mathcal{B}$, and, as our stability analysis shows, in this case, the stable stationary states are

$$I_+ = 0, \quad I_- = \frac{-\Gamma}{\mathcal{B}},$$

and

$$I_+ = \frac{-\Gamma}{\mathcal{B}}, \quad I_- = 0.$$

In numerical simulations, only a stable state can be observed as a stationary state, which explains why for the chosen β_n, we see the formation of either one or the other WS state.

When $\beta_n = \beta$, the ratio between $\mathcal{B}$ and $\tilde{\mathcal{B}}$ can be different. The coefficient $\tilde{\mathcal{B}}$ depends on the overlap of the intensity distributions of the states $W_{n\pm\tilde{m}}$, and this overlap decreases with increasing width of the WS state defined as

$$H = \sqrt{\sum_n W_n^2 (n - n_c)^2},$$

where n_c is the center of the WS state. Figure 5 shows the dependencies of $\mathcal{B}$ and $\tilde{\mathcal{B}}$ on the width of the states H (a state width H is determined by μ).

For $\mu = 0.2$ used in our direct modelling, the coefficients are $\mathcal{B} = 0.07$ and $\tilde{\mathcal{B}} = 0.04$. Therefore, in this case, there is only one stable stationary state

$$I_\pm = \frac{-\Gamma}{\mathcal{B} + \tilde{\mathcal{B}}}.$$

Thus, we can expect that in this case, the final state consists of two WS states of the same intensity, oscillating with different frequencies. This perfectly agrees with the results of our numerical simulations, see Fig. 4 c. In addition, for $\mu > 0.6$, there are regions where $\tilde{\mathcal{B}} > \mathcal{B}$, see Fig. 5 a. Hence, in these bands, there should be two stable states:

$$I_+ = 0, \quad I_- = \frac{-\Gamma}{\mathcal{B}},$$

and

$$I_+ = \frac{-\Gamma}{\mathcal{B}}, \quad I_- = 0,$$

instead of the previously observed single state. This is confirmed by numerical calculations.

We would like to note that the developed perturbation theory not only gives a qualitative explanation of the observed effect, but also allows determining the intensities of the two-component states with a good precision. The intensity $I_\pm(t)$ dependencies extracted from numerical simulations overlap with those calculated by formulas (8)–(9). For low linear gain a, the simulated and calculated results are in good agreement.

3. LASING WITH LINEAR GAIN IN SEVERAL RESONATORS

To increase the radiation power, it seems reasonable to introduce linear gain in several resonators. Let us first consider nonlinear losses present only in the pumped resonators. If the gain is uniformly distributed in the pumped resonators, we expect lasing to begin at lower pump amplitudes for a larger number of pumped resonators. Thus, Fig. 6 a shows the total energy E of the single-mode stationary state as a function of the pump amplitude a for different numbers of pumped neighbouring resonators M. In this figure, the stationary energy values E obtained via the perturbation method (solid line) and by numerical simulations (circles) are in good agreement for different M.

The single-frequency state is the only possible solution within the pump range $a_{th1} < a < a_{th2}$, where a_{th1} is the excitation threshold for the pair of WS modes with the fastest-growing amplitudes, and a_{th2} is the excitation threshold of the second fastest-growing pair. The simulations show that if the number of the pumped
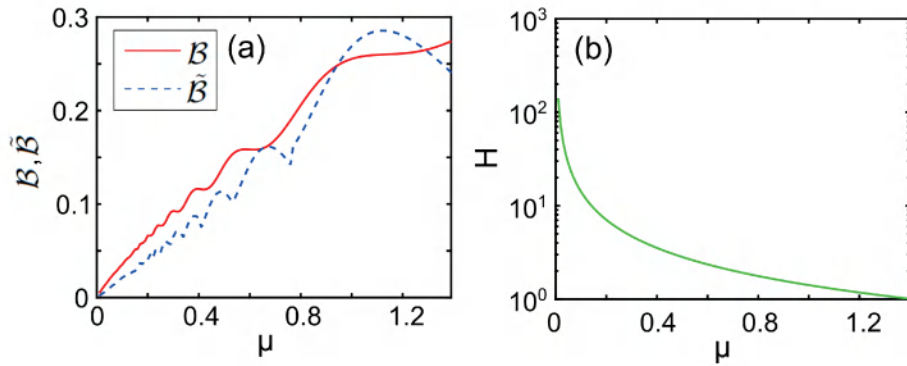
Fig. 5. (Color online) a — Dependencies of $\mathcal{B}$ and $\tilde{\mathcal{B}}$ on μ for spatially uniform nonlinear losses: $\beta_n = \beta = 1$. b — Dependence of the WS state width H on μ
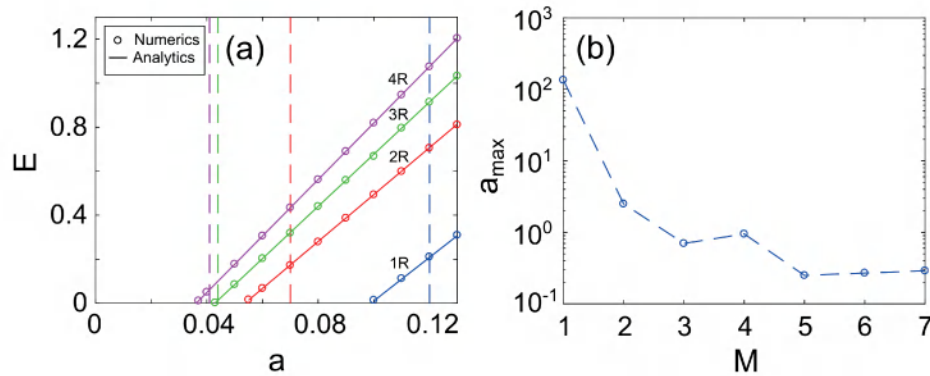

Fig. 6. (Color online) a — Total energy E of the single-mode stationary state as a function of the pump amplitude a obtained via the perturbation method (solid line) and by numerical simulation (circles) for different numbers of pumped adjacent resonators M: 1R, 2R, 3R and 4R. Dashed lines show the threshold pump amplitudes at which the next pair of Wannier–Stark states is excited. b — Maximum pump amplitude a_{max} providing single-frequency lasing vs. the number of pumped resonators M. Circles are analytical data, the dashed line is a guide for eyes. The nonlinear losses are nonzero only in the pumped resonators $\beta_M = \beta = 1$. The used parameters are: $\mu = 0.2$, $\gamma = 0.01$

resonators M increases, the range of the existence of a single-frequency solution narrows, see Fig. 6 a.

At sufficiently large pump amplitudes a, the single-frequency stationary state obviously becomes unstable and collapses. It is essential to study how the maximum pump amplitude a_{max} providing the single-frequency regime depends on the number of pumped resonators M. Figure 6 b shows this dependence: we can see that the critical pump amplitude decreases with increasing M. A possible reason is that for wide pumps, the overlap integrals defining the effective gain of modes weakly depend on the modes' indexes. Hence, the modes have very similar excitation thresholds. Thus, the single-frequency regime exists only in a small pump range between the excitation thresholds of the modes with the fastest and the second fastest-growing amplitudes.

Let us now consider in more detail the dynamics of the system when three neighbouring resonators are pumped. The numerical simulations show that near the threshold ($a \approx 0.043$), the radiation is monochromatic, see Fig. 6 a. Stationary states similar to those shown in Figs. 4 a and b are formed with equal probabilities.

When the pump amplitude exceeds the threshold value for the next pair of WS states ($a \approx 0.044$), a multi-frequency regime appears in the system. For pump slightly above this threshold, the stationary state can be seen as a superposition of two WS states with different frequencies. Due to nonlinearity, the temporal spectrum of the stationary state contains the entire set of frequency combinations, but for a weak nonlinearity, there are two dominating frequencies corresponding to the eigenfrequencies of the modes. Thus, this scenario
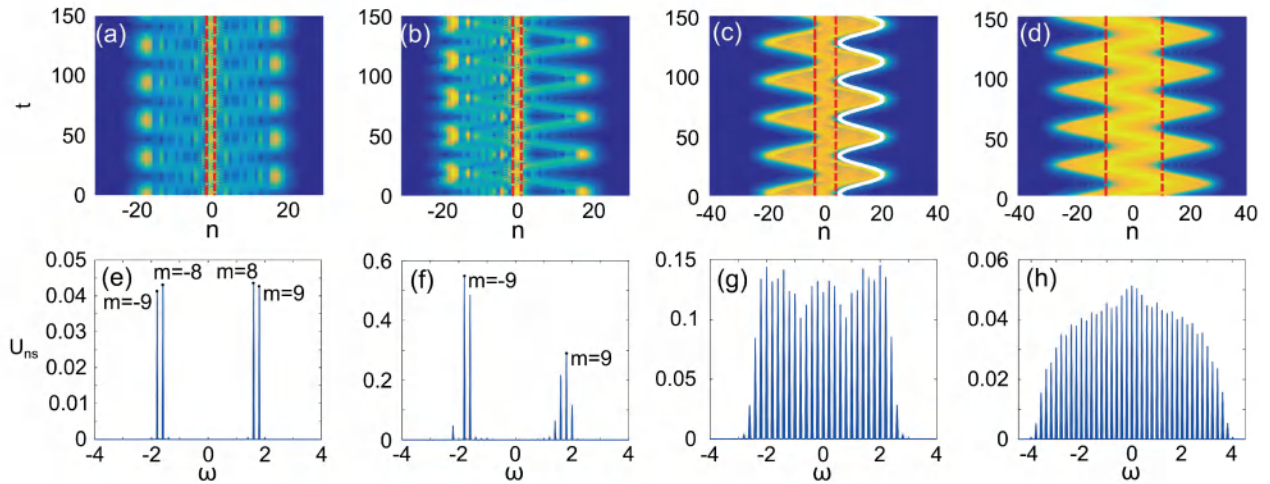
Fig. 7. (Color online) Evolution of the field module $|U_n(t)|$ and its spectrum, defined as $U_{n\,s}(\omega) = \sum_n |\int_{-\infty}^{\infty} U_n(t) \cdot e^{-i\omega t} dt|^2$, for the multi-frequency stationary state: $M = 3$, $a = 0.06\,(a, e)$; $M = 3$, $a = 0.2\,(b, f)$; $M = 7$, $a = 0.17\,(c, g)$; and $M = 21$, $a = 0.06\,(d, h)$. The dashed red lines show the pump area. In panel (c), the solid white line corresponds to Bloch oscillations in a linear conservative system. The nonlinear losses are nonzero only in the pumped resonators $\beta_M = \beta = 1$. The used parameters are: $\mu = 0.2$, $\gamma = 0.01$

is very similar to that with gain present in only one resonator and nonlinear losses in all the resonators of the system, see Fig. 4 c.

At higher pump levels, the multimode regime changes. Numerical simulations reveal that complex states resembling BOs appear, see Figs. 7 a, b. Their temporal spectra are shown in Figs. 7 e, f: there are four harmonics for the pump $a = 0.06$ corresponding to WS states with the indexes $m = \pm 8$ and $m = \pm 9$, see Fig. 7 e. For higher pumps, more temporal harmonics appear, see the spectrum for $a = 0.2$ in Fig. 7 f.

For pumps exceeding a threshold level ($a \approx 0.13$ for our parameters), the intensity distribution becomes asymmetric, compare Figs. 7 a and b. After the symmetry breaking, a pair of frequencies remains almost unchanged, but the other pair transforms into several spectral lines, indicating the excitation of many WS states. The winding patterns on the right in Fig. 7 b contain more harmonics, see Fig. 7 f, and thus, the BOs produced by the eigenstates in this part of spectrum become smoother.

For larger numbers of the excited resonators, the BOs become smoother and have a wider temporal spectrum, see Figs. 7 c, d, g, h showing the evolutions of the field amplitude and the temporal spectra for $M = 7$ and $M = 21$ excited resonators. To prove that the winding patterns in panels $(a)–(d)$ are related to BOs, we analytically calculated the trajectory of BOs for the linear conservative system and superimposed this curve

on Fig. 7 c. The amplitude and period of the BOs in the conservative counterpart of the considered system are very similar to those obtained from direct numerical simulations.

We verified that the multi-frequency regimes are qualitatively the same no matter if nonlinear losses are present in all the resonators or only in the excited ones. For this reason, we do not discuss the case of evenly distributed nonlinear losses in this paper.

4. MODE SELECTION

For practical purposes, increasing the pump range providing the single-frequency regime can be useful. This is especially important when the linear gain is created in many resonators, which allows increasing the output power of the working mode. To stabilize the single-frequency regime, we suggest profiling the pump. Profiling provides control over the effective gain for different modes, and thus allows one of the modes to have an increment significantly higher than that of the other modes.

We start with a positive linear gain only in one resonator; this resonator also has nonlinear losses. As we discussed above, in this case, two different WS states can be formed with equal probability. Let us show that by choosing an appropriate pump, we can ensure that stationary states are predefined by the gain shape and thus do not depend on the initial conditions. For
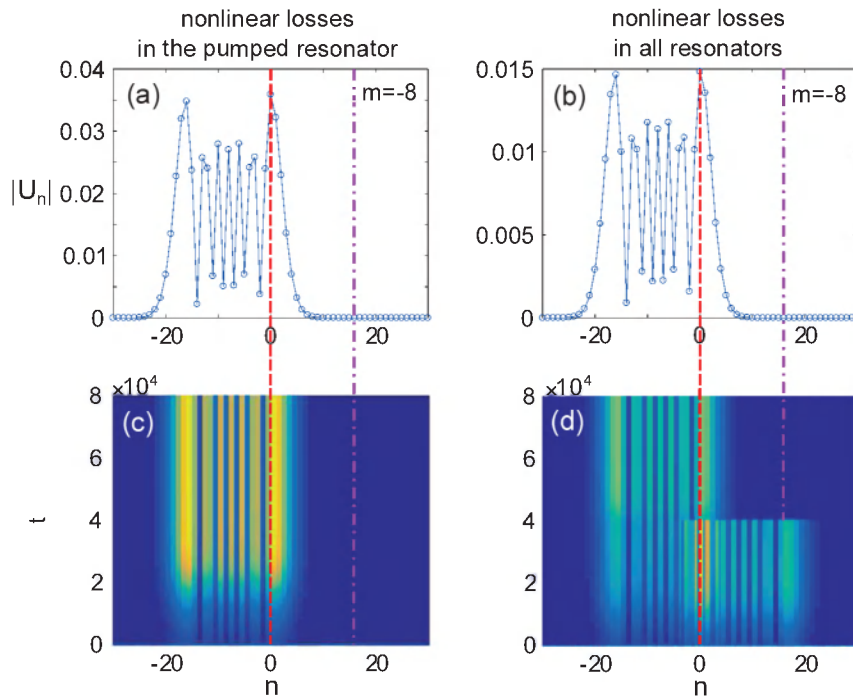
Fig. 8. (Color online) Evolutions of the field amplitude $|U_n(t)|$ and stationary distribution of the amplitudes for negative linear losses $\gamma_0 = \gamma - a$ only in the resonator with $n = 0$ and additional losses $\tilde{\gamma}$ introduced to the resonator with $n = 16$, so that $\gamma_{16} = \gamma + \tilde{\gamma}$. Nonlinear losses are nonzero only in the excited resonator with $n = 0$, i.e., $\beta_0 = \beta$ for (a), (c); nonlinear losses are spatially uniform, i.e., $\beta_n = \beta$ for (b), (d). Panels (c, d) show evolutions from weak noise, and panels (a, b), the final distribution of the amplitudes. The blue circles correspond to the resonators, the solid blue lines are guides for eyes. The red dashed line marks the resonator with the gain, the dash-dotted magenta line shows the additional losses introduced for mode selection. For nonlinear losses present in all resonators, there are no additional losses at $t < 4 \cdot 10^4$. The formation of the hybrid state consisting of two WS states is shown in (d). The additional losses are switched on at $t = 4 \cdot 10^4$ in the resonator $n = 16$, suppressing one of the WS states, and the stationary state becomes a single-frequency one, with the amplitude profile corresponding to the fastest-growing WS state, see panel (b). The used parameters are: $\mu = 0.2$, $\gamma = 0.01$, $\tilde{\gamma} = 0.03$, $a = 0.1$, $\beta = 1$

this, we modify the effective losses in the individual resonators by adding some additional losses to a certain resonator, see Figs. 8 a, c, showing the distribution of the effective losses.

Without the added losses, there are two eigenmodes with the same effective linear gain, but different frequencies and field distributions. Then, we increase the losses in the resonator where one of the modes has an intensity maximum, but the other mode has a low intensity. The added dissipation suppresses the effective linear gain of the first mode, but barely affects the growth rate of the second mode. As a consequence, we can achieve a controllable excitation of the desirable WS state. The evolution of the mode growing from weak noise is shown in Figs. 8 a, c.

In Sec. 2, we have shown that if there are nonlinear losses in all the resonators, the stationary state is a combination of two WS states with the fastest-growing amplitudes and different frequencies. By introducing

additional losses into one of the resonators, we can suppress one of the WS states. Therefore, a modification of the pump profile can provide single-frequency lasing. This is illustrated in Figs. 8 b, d, showing the field evolution with weak-noise initial conditions. For $t < 4 \cdot 10^4$, there are no additional losses, and a stationary state is formed as a superposition of two WS states. At $t = 4 \cdot 10^4$, we switch on additional losses in the resonator $n = 16$, immediately suppressing one of the WS states, and a stable single-frequency WS state is observed.

To increase the lasing mode power, it is natural to increase the area and intensity of the pump. But, as we discussed above, this makes single-mode regime difficult to observe. However, nonlinear losses located in the excited resonators hamper single-frequency generation especially strongly. This issue can be overcome by gain profiling: pumping only the resonators in which the working mode has intensity maxima and adding
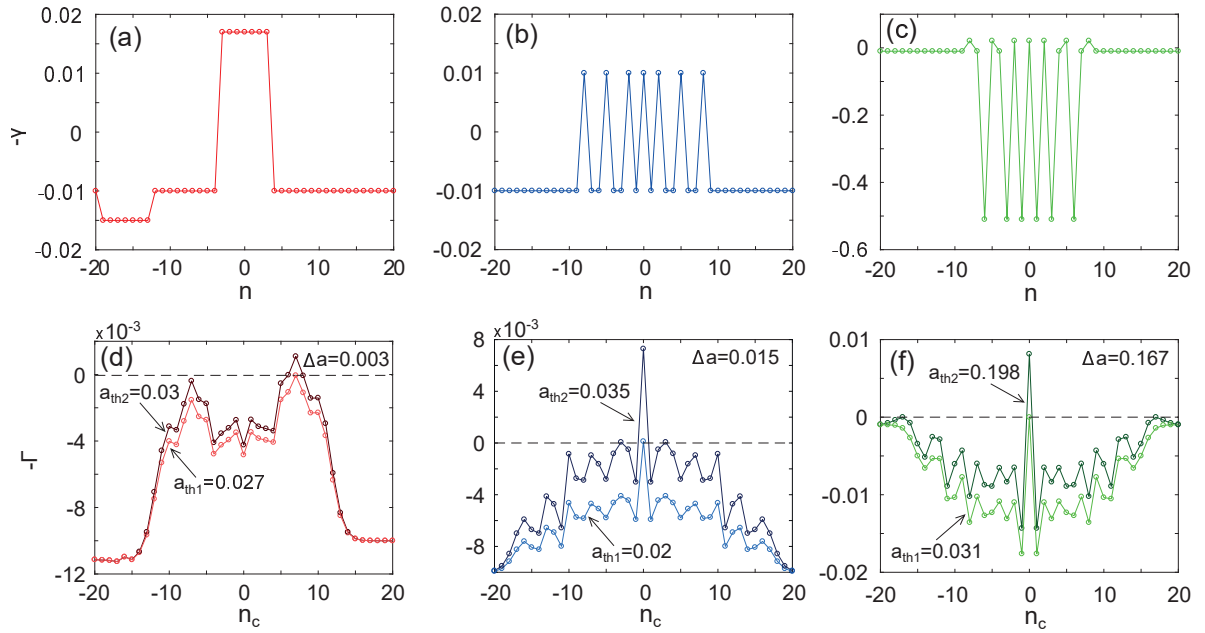
Fig. 9. (Color online) Gain profiles $-\gamma_n$ with a pump amplitude just above the lasing threshold: $a = 0.027$ (a), $a = 0.02$ (b), $a = 0.031$ (c). Additional losses are $\tilde{\gamma} = 0.005$ in (a) and $\tilde{\gamma} = 0.5$ in (c). The circles correspond to the resonators, the solid lines are guides for eyes. d–f — Effective linear gain $-\Gamma$ as a function of the Wannier – Stark state center position n_c for the two first threshold pump amplitudes $a_{th1,2}$ for the gain distributions (a)–(c), respectively. The circles correspond to the data from the perturbation method, the solid lines are guides for eyes. The used parameters are: $\mu = 0.2$, $\gamma = 0.01$

losses to the resonators where the other, undesirable modes have a large intensity. In numerical simulations, we consider 7 pumped oscillators and different distributions of the effective losses, see Figs. 9 a–c.

The effective gain created by these pumps depends on the index of the WS state, which is shown in Figs. 9 d–f. There, the effective gain for one of the modes is much greater than the gain for the other modes, see panels (e, f). Moreover, in a wide range of pump amplitudes, only one mode has a positive increment. Thus, the mode with the fastest-growing amplitude is expected to define the stationary state.

We used numerical simulations to test the hypothesis that if only one mode has a positive increment, then the final stationary state is a single-frequency one. Numerical simulations fully confirm this prediction. At the same time, as expected, for the pump profile shown in Fig. 9 a, the single-frequency generation range is extremely small ($E_{max} = 0.04$).

However, in simulations, due to gain profiling, single-frequency lasing regimes are maintained even at sufficiently high pumps, where there are more than one growing mode. Thus, if we pump only the resonators in which the working mode has intensity maxima, see Fig. 9 b, the existence range of the single-

frequency regime increases by two orders of magnitude ($E_{max} \approx 4$). This behavior can be explained by the fact that this pump profiling provides a better selection of the working mode in terms of the effective gain difference, see Fig. 9 e.

Single-frequency range can be increased even further by introducing additional losses to the resonators where the intensity of the working mode has minima, see the pump profile shown in Fig. 9 c. In this case, it is interesting to study how the maximum values of the pump amplitude and the energy of the single-mode stationary state depend on the level of additional losses $\tilde{\gamma}$. The numerical results are demonstrated in Fig. 10: the pump range in which the lasing is monochromatic drastically increases with $\tilde{\gamma}$ (by an order of magnitude). Hence, the maximum achievable energy of the working mode is much higher if additional losses are included. Besides, a comparison of panels (a) and (b) shows that the energy of single-frequency state depends almost linearly on the pump amplitude. We should also note that for a pump amplitude $a > 3$, single-mode regime is still supported, but the dissipative terms become comparable to the conservative ones, and therefore the modes in the system are no longer purely WS states.
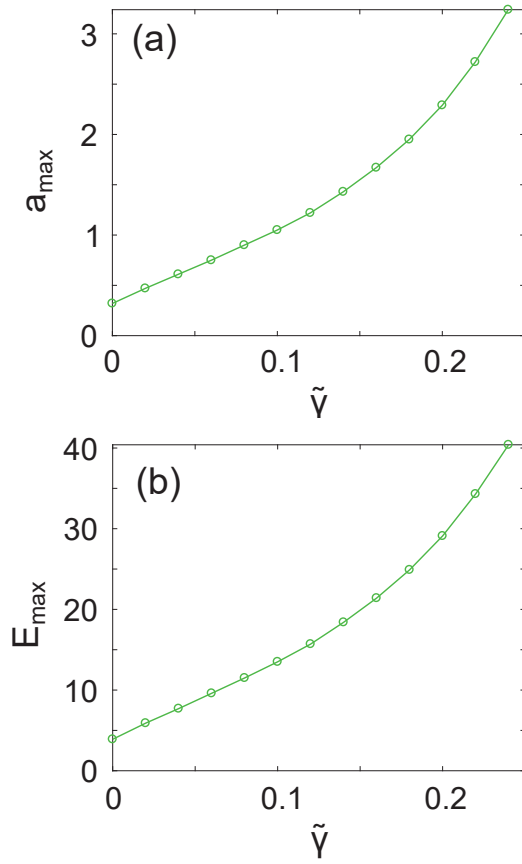
Fig. 10. (Color online) Maximum pump amplitude a_{max} (a) and maximum total energy E_{max} (b) allowing single-frequency lasing regime vs. the additional losses value $\tilde{\gamma}$ for the gain profile shown in Fig. 9 c. The circles are numerical data, and the solid lines are guides for eyes. Nonlinear losses are nonzero only in the pumped resonators $\beta_M = \beta = 1$. The used parameters are: $\mu = 0.2$, $\gamma = 0.01$

5. CONCLUSION

In this paper, we have studied the dynamics of Wannier – Stark (WS) states in a discrete system, an array of interacting optical resonators. Linear gain in some of the resonators can switch the system to lasing regime, provided that the gain exceeds a threshold value depending on the structure of the WS state and the spatial distribution of the pump. The linear gain is saturated by the nonlinear losses so that stationary states can form in the system. In the suggested system, the lasing modes are shown to be WS states. We considered a system with nonlinear losses only in the pumped resonators having linear gain (only these resonators are appropriately doped) and a system with nonlinear losses present in all the resonators (all the resonators are doped, but an external pump profile cre-

ates linear gain as a function of resonator index).

To study the dynamics of the system analytically, we developed a simple perturbation theory and used it to find the excitation thresholds and stationary amplitudes, and to explain the mode competition. The comparison of the perturbation theory with the results of direct numerical simulation shows that the perturbation theory works well if the dissipative terms are small, i.e. they do not significantly affect the structure of the eigenmodes, but govern the dynamics of the complex amplitudes of the modes.

We reveal that the nonlinear losses distribution can seriously affect the dynamics of the excited WS states. In particular, we show that for linear gain only in one resonator, single-frequency lasing occurs in the vicinity of the lasing threshold if nonlinear losses exist only in the pumped resonator. However, if there are nonlinear losses in all resonators, then even in the vicinity of the lasing threshold, the stationary state is multi-frequency, with two dominating spectral lines corresponding to the frequencies of the two WS states with the maximum linear growth rate. To explain this effect, we have calculated the coefficients determining the nonlinear interaction between the modes. This analysis shows that in the first case, the mode with a higher amplitude successfully suppresses its competitor, but in the second case, this suppression is insufficient to prevent the excitation of the other mode.

We also consider linear gain present in several neighboring resonators and show that single-frequency lasing is still possible in the vicinity of the lasing threshold. However, this regime occurs only within a small pump range, and the energy of the lasing mode is low. If the pump amplitude grows, a complex multi-frequency regime is formed. Using such a pump, Bloch oscillations (BOs) can be generated in the dissipative system. At relatively low pump amplitudes, evolution of intensity distribution has a symmetric winding pattern, which indicates BOs. For higher pumps, symmetry breaks, and the evolution seems to indicate two different coexisting BOs.

We also study the problem of stabilization of single-frequency lasing. By choosing an appropriate pump profile, it is possible to extend the single-frequency regime and significantly increase the lasing mode energy. By introducing additional losses to the system, we can achieve an even better selection of the working mode and thus realize single-frequency lasing of the chosen WS mode in a wide pump range.

To summarize, we have examined for the first time the generation of WS states in microlaser arrays. The lasing mode has a wide profile, covering many excited

resonators, which allows pump to create gain in many cavities. This way, the maximum power of the emitted radiation can be increased. In addition, we show that a single WS state can be excited by an appropriate pump, enabling single-frequency lasing. Remarkably, the WS frequencies depend on their position, and therefore, the lasing frequency can be tuned by moving the pump position. Moreover, all the WS states have the same spatial structure, and thus, frequency tuning does not affect the profile of the lasing mode. Speaking of tunability, it is worth mentioning that the discussed systems can be efficiently controlled by suitable heating of the sample [47]. This opens an additional opportunity for the fine tuning of the lasing frequency. Thus, our work demonstrates a promising way to obtain coherent radiation with a wide lasing mode, which can potentially be applied in various laser devices.

REFERENCES

1. T. Higuchi, M. I. Stockman, and P. Hommelhoff, Phys. Rev. Lett., **113**, 213901 (2014).

2. H. Y. Wang, X. M. Zhao, L. Zhuang et al., J. Phys.: Condens. Matter, **34**, 365402 (2022).

3. U. B. Hansen, O. F. Syljuåsen, J. Jensen et al., Nature Communications, **13**, 2547 (2022).

4. G.H. Wannier, Elements of solid state theory, CUP Archive (1959).

5. W. Shockley, Phys. Rev. Lett., **28**, 349 (1972).

6. F. Bloch, Z. Phys., **52**, 555 (1929).

7. C. Zener, Proc. R. Soc. A, **145**, 523 (1934).

8. W.V. Houston, Phys. Rev., **57**, 184 (1940).

9. C. Waschke, H.G. Roskos, R. Schwedler et al, Phys. Rev. Lett. **70**, 3319 (1993).

10. M.B. Dahan, E. Peik, J. Reichel et al., Phys. Rev. Lett., **76**, 4508 (1996).

11. S. Wilkinson, C. Bharucha, K. Madison et al., Phys. Rev. Lett., **76**, 4512 (1996).

12. H. R. Zhang and C. P. Sun, Phys. Rev. A, **81**, 063427 (2010).

13. Z.A. Geiger, K.M. Fujiwara, K. Singh et al., Phys. Rev. Lett., **120**, 213201 (2018).

14. Z. Pagel, W. Zhong, R.H. Parker et al., Phys. Rev. A, **102**, 053312 (2020).

15. L. Masi, T. Petrucciani, G. Ferioli et al., Phys. Rev. Lett., **127**, 020601 (2021).

16. S. Longhi, Opt. Lett., **30**, 786 (2005).

17. S. Bahmani and A.N. Askarpour, Phys. Lett. A, **384**, 126596 (2020).

18. G. Monsivais and R. Esquivel-Sirvent, Journal of Mechanics of Materials and Structures, **2**, 1585 (2007).

19. G. Monsivais, R. Mendez-Sanchez, A. de Anda et al., Journal of Mechanics of Materials and Structures, **2**, 1629 (2007).

20. N. Lanzillotti-Kimura, A. Fainstein, B. Perrin et al., Phys. Rev. Lett., **104**, 197402 (2010).

21. Y.-K. Liu, H.-W. Wu, P. Hu et al., Appl. Phys. Express, **14**, 064501 (2021).

22. A.R. Davoyan, I.V. Shadrivov, A.A. Sukhorukov et al., Appl. Phys. Lett., **94**, 161105 (2009).

23. V. Kuzmiak, S. Eyderman, and M. Vanwolleghem, Phys. Rev. B, **86**, 045403 (2012).

24. B. H. Cheng, Y. C. Lai, and Y. C. Lan, Plasmonics, **9**, 137 (2014).

25. V. Kuzmiak, A. A. Maradudin, and E. R. Mendez, Opt. Lett., **39**, 1613 (2014).

26. A. Block, C. Etrich, T. Limboeck et al., Nature Communications, **5**, 3843 (2014).

27. H. Wetter, Z. Fedorova, and S. Linden, Opt. Lett., **47**, 3091 (2022).

28. H. Flayac, D. D. Solnyshkov, and G. Malpuech, Phys. Rev. B, **83**, 045412 (2011).

29. H. Flayac, D. D. Solnyshkov, and G. Malpuech, Phys. Rev. B, **84**, 125314 (2011).

30. J. Beierlein, O.A. Egorov, T.H. Harder et al., Adv. Opt. Mater., **9**, 2100126 (2021).

31. G. Monsivais, M. del Castillo-Mussot, and F. Claro, Phys. Rev. Lett., **64**, 1433 (1990).

32. C. M. de Sterke, J. E. Sipe, and L. A. Weller-Brophy, Opt. Lett., **16**, 1141 (1991).

33. U. Peschel, T. Pertsch, and F. Lederer, Opt. Lett., **23**, 1701 (1998).

34. A. Kavokin, G. Malpuech, A. Di Carlo et al., Phys. Rev. B, **61**, 4413 (2000).

35. G. Malpuech, A. Kavokin, G. Panzarini et al., Phys. Rev. B, **63**, 035108 (2001).

36. S. Longhi, Europhys. Lett., **76**, 416 (2006).

37. R. El-Ganainy, K. G. Makris, M. A. Miri et al., Phys. Rev. A, **84**, 023842 (2011).

38. G. Lenz, I. Talanina, and C. M. De Sterke, Phys. Rev. Lett., **83**, 963 (1999).

39. U. Peschel, C. Bersch, and G. Onishchukov, Open Phys., **6**, 619 (2008).

40. P. B. Wilkinson, Phys. Rev. E, **65**, 056616 (2002).

41. S. Longhi, Phys. Rev. Lett., **103**, 123601 (2009).

42. N. K. Efremidis, and D. N. Christodoulides, Opt. Lett., **29**, 2485 (2004).

43. C. M. de Sterke, J. N. Bright, P. A. Krug et al., Phys. Rev. E, **57**, 2365 (1998).

44. M. Ghulinyan, C. J. Oton, Z. Gaburro et al., Phys. Rev. Lett., **94**, 127401 (2005).

45. X. Qi, K. G. Makris, R. El-Ganainy et al., Opt. Lett., **39**, 1065 (2014).

46. S. Mukherjee, A. Spracklen, D. Choudhury et al., New J. Phys., **17**, 115002 (2015).

47. T. Pertsch, P. Dannberg, W. Elflein et al., Phys. Rev. Lett., **83**, 4752 (1999).

48. R. Morandotti, U. Peschel, J. S. Aitchison et al., Phys. Rev. Lett., **83**, 4756 (1999).

49. R. Sapienza, P. Costantino, D. Wiersma, et al., Phys. Rev. Lett., **91**, 263902 (2003).

50. V. Agarwal, J. A. del Rio, G. Malpuech et al., Phys. Rev. Lett., **92**, 097401 (2004).

51. S. Longhi, M. Lobino, M. Marangoni et al., Phys. Rev. B, **74**, 155116 (2006).

52. B. A. Usievich, V. A. Sychugov, J. K. Nirligareev et al., Opt. Spectrosc., **97**, 790 (2004).

53. N. Chiodo, G. Della Valle, R. Osellame et al., Opt. Lett., **31**, 1651 (2006).

54. A. Regensburger, C. Bersch, M. A. Miri et al., Nature, **488**, 167 (2012).

55. Y. L. Xu, W.S. Fegadolli, L. Gan et al., Nature Comm., **7**, 11319 (2016).

56. I.L. Garanovich, S. Longhi, A.A. Sukhorukov et al., Phys. Rep., **518**, 1 (2012).

57. X. Yang, C. Gong, C. Zhang et al., Laser & Photonics Rev., **16**, 2100171 (2022).

58. Z. Chen, G. Dong, G. Barillaro et al., Progress in Materials Science, **121**, 100814 (2021).

59. A. E. Zhukov, N. V. Kryzhanovskaya, E. I. Moiseev et al., Light: Science & Applications, **10**, 80 (2021).

60. Q. Zhang, Q. Shang, R. Su et al., Nano Lett., **21**, 1903 (2021).

61. M. Sumetsky, Progress in Quantum Electronics, **64**, 1 (2019).

62. H. He, H. Li, Y. Cui et al., Adv. Opt. Mater., **7**, 1900077 (2019).

63. Y. Zhao, Y. Chen, Z. S. Hou et al., Opt. Lett., **47**, 617 (2022).

64. K. Koshelev, S. Kruk, E. Melik-Gaykazyan et al., Science, **367**, 288 (2020).

65. M. S. Hwang, K. Y. Jeong, J. P. So, et al., Comm. Phys., **5**, 106 (2022).

66. D. Bajoni, P. Senellart, E. Wertz et al., Phys. Rev. Lett., **100**, 047401 (2008).

67. A. Verbitskiy, A. Yulin, and A. G. Balanov, Phys. Rev. A, **107**, 053519 (2023).

68. W. Deering, M. Molina, and G. Tsironis, Appl. Phys. Lett., **62**, 2471 (1993).

69. J. Eilbeck, G. Tsironis, and S. K. Turitsyn, Phys. Scr., **52**, 386 (1995).

70. P.G. Kevrekidis, K.O. Rasmussen and A.R. Bishop, International Journal of Modern Physics B, **15**, 2833 (2001).

71. N.K. Efremidis, S. Sears, D.N. Christodoulides et al., Phys. Rev. E, **66**, 046602 (2002).

72. A.A. Sukhorukov, Yu.S. Kivshar, H.S. Eisenberg et al., IEEE J. Quantum Electron., **39**, 31 (2003).

73. U. Peschel, O. Egorov, and F. Lederer, Opt. Lett., **29**, 1909 (2004).

74. D. Pelinovsky and P. G. Kevrekidis, Physica D, **212**, 1 (2005).

75. A. Yulin, D. V. Skryabin, and P. St. J. Russell, Opt. Express, **13**, 3529 (2005).

76. A.V. Yulin, D.V. Skryabin, and A.G. Vladimirov, Opt. Express, **14**, 12347 (2006).

77. H. Susanto, P. G. Kevrekidis, B. A. Malomed et al., Phys. Rev. E, **75**, 056605 (2007).

78. O.A. Egorov and F. Lederer, Phys. Rev. A, **76**, 053816 (2007).

79. O.A. Egorov, F. Lederer, and Yu.S. Kivshar, Opt. Express, **15**, 4149 (2007).